Shear Stress Statistics in a Compound Channel Flow

W. Czernuszenko, P. M. Rowiński

Institute of Geophysics, Polish Academy of Sciences, Księcia Janusza 64, 01-452 Warszawa, Poland,
e-mail: wczer@igf.edu.pl

Abstract

The results of comprehensive measurements of three-dimensional turbulent velocities carried out in a laboratory compound channel are presented. Tests were performed in a two-stage channel with a smooth main channel bed consisting of concrete and rough floodplains and sloping banks. Instantaneous velocities were measured with the use of a three-component acoustic Doppler velocimeter. The main aim of the study is the recognition of structure of Reynolds stresses in turbulent open channel flows. Particular attention has been paid to bursting events such as ejections and sweeps. The bursting phenomenon occurs originally near the buffer layer and then shows a coherent or organized flow structure during its convection process.

The probability density distributions of the turbulent velocities were measured at different distances from the bed in the main channel and also above the inclined walls. In the main channel, the lateral turbulent velocity is seen to follow the normal Gaussian distribution more closely than the remaining two components. Above the inclined walls, all distributions turned out to have greater skewness. The probability density distributions of correlations between velocity fluctuations were also calculated. These distributions have long tails and sharp peaks and fit the theoretical distributions very well. The structure of instantaneous Reynolds stresses was analyzed by a quadrant technique with an arbitrarily chosen threshold level. It has been shown that the largest contribution to turbulent stresses comes from the second quadrant (ejection) and the fourth quadrant (sweep). The basic temporal characteristics for quadrant events, like the average and maximum time for a zero hole size, have been determined in the study. Calculations of maximum duration times for all events reveal that times are greater for even quadrants than for odd quadrants.

Key words: open channel, turbulence, measurements, Reynolds stresses, coherent structures

Notation

D	–	excess or kurtosis,
$E[\ ]$	–	represents the expected value,
H	–	threshold level,
k	–	number of particular events, k_i,
K_0	–	zeroth-order modified Bessel function of the second kind,
$L_{i\,\max}$	–	largest sizes of ejection and sweep,

N	–	total number of observations,
$n_{i,k}$	–	number of occurrences in the sequence of events belonging to a particular quadrant,
$NRS(uw)$	–	normalized instantaneous Reynolds-stress,
NRS_{total}	–	normalized total Reynolds stresses for a particular component of Reynolds stress tensor,
$p(u)$	–	probability density function,
$P_i = (T_{i,k}/T)$	–	frequency of appearance of each quadrant,
$QD - i$	–	notation for i-quadrant,
R	–	correlation coefficient,
rms	–	root mean square,
RS_i	–	fractional Reynolds stress for a particular component of Reynolds stress tensor belongs to the i-quadrant,
RS_{total}	–	total Reynolds stresses for a particular component of Reynolds stress tensor,
S	–	skewness,
$t = t_0$	–	beginning of data measurement,
T	–	total measuring time,
T_i	–	total time of occurrences of particular event,
$T_{i,k} = (n_{i,k}\Delta t)$	–	period of time for k sequence of i-quadrant,
$T_{i,\max}$	–	maximum length of sequence belongs to i-quadrant $T_{i,k}$,
$T_{i,\min}$	–	minimum length of sequence belongs to i-quadrant $T_{i,k}$,
$u(t)w(t)$	–	product of two turbulent velocities = covariance term (event) or term proportional to instantaneous shear stress,
Δt	–	a period of time in which velocity is measured.

1. Introduction

Analysis of a flow turbulence structure cannot be considered complete if it does not comprise all information on the existing coherent structures. There have been extensive investigations of turbulent flow conditions in a variety of compound channels; among them the structure of turbulence in the laboratory flume of Warsaw University of Life Sciences occupies an important place in professional literature. These studies have comprised both one-dimensional (Rowiński et al 2002) and three-dimensional measurements (Czernuszenko et al 2007); the structure of turbulence when vegetation was placed on floodplains was also considered (Rowiński and Mazurczyk 2006). All of the studies lacked, however, basic information on coherent structures existing in the flow.

The presence of coherent structures in turbulent shear flows is a form of proof that some order exists in apparently random flows. Their particular role in open channel flows is associated with momentum and scalar transport (like temperature, pollution or sediment concentrations etc.). The occurrence of coherent structures

was revealed by flow visualization techniques employing hydrogen bubbles quite a long time ago (e.g. Grass et al 1993, Lu and Willmarth 1973, Nakagawa and Nezu 1977). A few models of those structures have been proposed and new vortical structures have been introduced like arch or horseshoe vortex, hairpin vortex, low-speed streak, burst and sweep events (for details see Offen and Kline 1975, Kumar et al 1998). It has been established that the low-velocity streaks in the sublayer, and the subsequent ejection of the low-velocity fluid to the outer region of the flow are important characteristics of the near-wall region. Considerable experimental work has been done in the last few years to detect those structures with single-point velocity measurements. A number of algorithms have been also proposed allowing for the detection of such structures as VITA, Quadrant, U-level or TPVA (Lu and Willmarth 1973, Bogard and Tiederman 1986, Hurther 2000). Recently, Franca and Lemmin (2006) have combined the conditional sampling technique and the wavelet multilevel decomposition of single point instantaneous velocity measurements.

From the classic experimental work of Lu and Willmarth (1973) performed in a wind tunnel, we learn that when the turbulent vertical velocity at the edge of the viscous sublayer diminishes, ejections occur. Sweeps occur when this velocity increases above a certain threshold. The ejections turned out to be the largest contributors to the total Reynolds stresses (77%) and the sweeps are the second largest (55%) among all possible events. The excess percentage over 100% is due to other small negative contributions.

Keshavarzy and Ball (1977) undertook their experiments in a tilting rectangular flume and they found that the shear stresses applied to the sediment particles on the bed resulting from the sweep events depend on the magnitude of the turbulent stresses and their probability distributions. They concluded that for sweeps, the mean shear stress is approximately 140% of the overall temporal mean shear stress near the bed and it increased to approximately 200% near the water surface. A similar result was obtained for ejections. The frequency of sweeps and ejections events appeared to be approximately 30%, whereas the remaining events constituted only 20% near the channel bed.

Nakagawa and Nezu (1981) in their experiments, conducted in a 2-D, fully developed turbulent flow in a smooth, open channel at water flow depth of about 8 cm, investigated the structure of space-time correlations of bursting motions by conditional sampling analysis of instantaneous Reynolds-stress signals measured by two dual sensor hot-film probes. They concluded that the spatial and time scale of the sweep motion are larger than those of the ejection motion, and that the spatial scale of the ejection motion extend more widely downstream than upstream, and the other way round in the case of the sweep motion.

Bogard and Tiederman (1986) tested as many as seven different detection algorithms in their measurements of water flow. The major conclusion of this study is that the Quadrant technique applied to single-point velocity measurements are able to detect bursts. Other algorithms are significantly less accurate than the Quadrant

technique. The effectiveness of those algorithms depend on the so-called threshold levels and the optimum threshold for the Quadrant technique was found to be about 1.

Hurther (2000) has measured the 3-D instantaneous velocity profiles at the center of uniform, turbulent open-channel flows over smooth and rough beds covered with sand with a mean grain size 1.7 mm. The quadrant fractional method showed that in the outer region of boundary layer ($z/h > 0.2$), ejections have greater influence than sweeps, but in the inner region, the sweep contribution increases and reaches the same level as the ejections. The effect of bottom roughness in changing the balance between ejections and sweeps is important below 0.2 h.

Coherent flow structures have an impact on numerous phenomena in rivers, among them on sediment transport. For example, Sumer and Deigaard (1981) demonstrated that ejection events are responsible for saltation movements of particles in the inner flow region. The majority of sediment transport models based on coherent flow structures dynamics consider that ejection events are the most relevant structures in particle entrainment. The principle of these models is based on geometric and kinematic characteristics of the ejections. When the ejection starts to lose its coherence, the particles are released and start to settle down towards the bed at a velocity depending on their size and density and the state of turbulence. The mean suspended travel time of the particles corresponds to the mean lifetime of ejection events. The mean longitudinal distance of the travel distance is in agreement with the characteristic wavelength of the ejection in clear water.

In recent years literature studies on coherent structures have significantly increased in number and have been performed in both laboratory flumes (e.g. Detert et al 2007), as well as in natural channels (e.g. Nikora and Goring 2000, Roy et al 2004). At the fore front of our interests for this study is the detection of coherent structures in compound channels, a subject of intensive research all over the world (e.g. Hyun et al 2003, Prooijen et al 2005). The present study aims at the analysis of measurements of 3D turbulent velocities carried out in a laboratory compound channel. Tests were performed in a two-stage channel with a smooth main channel bed and with rough floodplains and sloping banks. Instantaneous velocities were measured with use of a three-component acoustic Doppler velocity meter (ADV). An emphasis was put on the analysis of instantaneous Reynolds-stresses. Particular attention has been paid to bursting events such as ejections and sweeps as well as the calculation of mean and maximum duration time for all events. Preliminary results of the study have been presented in Czernuszenko and Rowiński (2008).

2. Experimental Set-up

A detailed description of the measuring techniques used and detailed consideration of basic properties of turbulence in the considered flow are given in Czernuszenko et al (2007). The experiments were carried out in a concrete flume, 16 m long

and 2.10 m wide with symmetrically complex trapezoidal cross-section. The bed slope of the channel was 0.5‰. A row of PCV pipes was installed in the initial channel reach to subside the stream. One cross-section in the middle of the flume was selected for velocity measurements (Fig. 1). It consisted of 23 verticals – six on each floodplain and eleven in the main channel.
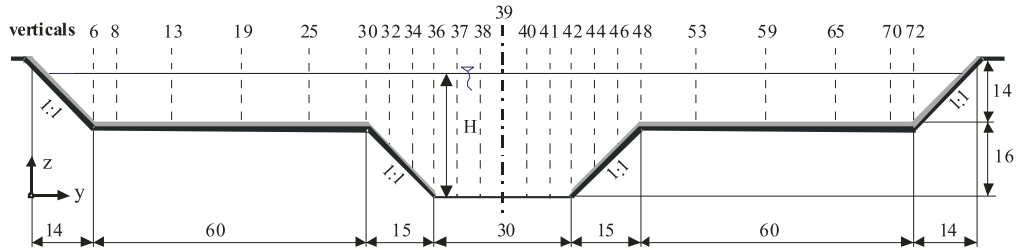

Fig. 1. Scheme of the experimental cross-section with measuring verticals: H is the water depth

Water levels in the main channel and on the floodplains, all three components of point velocities, water temperature and water discharge were measured throughout the course of the experiment. Water depth in the channel was recorded by means of a needle level gauge. Instantaneous velocities were measured with the use of a three-component acoustic Doppler velocity meter (ADV) manufactured by Sontek Inc. The acoustic sensor was mounted on a rigid stem attached to a specially designed trolley allowing for precise positioning. ADV works on pulse-to-pulse coherent Doppler techniques in relatively high temporal resolution (Lohrmann et al 1994). ADV proved to yield a good description of turbulence characteristics when certain conditions related to the flow itself and the configuration of the instrument are satisfied. The measurements were conducted with a maximum frequency of 25 Hz in the velocity range of 0 to 1.0 m/s with the accuracy of 0.25 cm/s. Sampling volume was equal to 0.1 cm^3. Buffin-Bélanger and Roy (2005) report that, for the most turbulent statistics, a sufficient record length for the measurements is 60–90 s. In cases of our experiments even longer time series (120–360 s) were recorded to provide reliability of data and constancy of higher order velocity moments. Both down-looking sensor orientation and side-looking probes (close to the water surface, less than 6 cm in order to avoid flow interference) were utilized during the measurements.

Water discharges were recorded with the use of a measuring circular overfall – 540 mm in diameter. During the experiment $Q = 95.20$ l/s. Water surface slope was measured by recording the pressure differences among piezometers located along the centerline of the channel bed at distances of 4 and 12 m from the channel entrance. The surface of the main channel bed was smooth (Manninig roughness coefficient $n = 0.011$ m$^{-1/3}$s) and made of concrete, while the floodplains and sloping banks

were covered by cement mortar composed of terrazzo with grains of 0.5 to 1 cm in diameter ($n = 0.018$ m$^{1/3}$s). The water depth in the main channel was kept at the level of $H = 28.3$ cm and on the floodplains $h = 12.3$ cm. The main channel width was equal to 28 cm and the floodplains width was 60 cm. The sloping banks were inclined at an angle of 1:1.

3. Statistical Properties of Turbulent Velocities: Basic Definitions

3.1. Probability Density Function of Turbulent Velocity

Each component of turbulent flow velocities at any point is a random variable. Its behaviour can be described by a probability density function (pdf), which may be characterized by statistical moments of different orders which can be relatively easily obtained from experiments. A statistical moment of n-th order for longitudinal velocities (analogous definitions apply to other components as well) collected at one point can be defined by the following formula:

$$E[u^n] = \int_{-\infty}^{\infty} u^n p(u) du, \tag{1}$$

where $E[\ ]$ represents the expected value, $p(u)$ is the pdf, and $n = 1, 2, 3 \dots$ For a stationary, ergodic process, $E[u^n]$ is simplified to the form:

$$E[u^n] = \overline{u^n} = \lim_{T \to \infty} \frac{1}{T} \int_{t_0}^{t_0+T} u^n dt, \tag{2}$$

where the overbar indicates a time-averaged value, $t = t_0$ at the beginning of the data series being analyzed, and T = duration of the data. It is assumed that all our data series are stationary ergodic processes, therefore Eq. (1) holds and will be applied in this study.

The probability density function and its main statistical characteristics of all three components of non-dimensional turbulent velocities (scaled by rms value) have been calculated. The main characteristics are related to the first four statistical moments, i.e. mean, root mean square (rms), skewness, and excess or kurtosis. For the convenience of the reader let us state the well-known definitions for longitudinal component of the velocity vector:

$$u_{rms} \equiv u' = \sqrt{\overline{u^2}}, \quad S_u = \frac{\overline{u^3}}{u'^3}, \quad D_u = \frac{\overline{u^4}}{u'^4} - 3. \tag{3}$$

All of those characteristics for the given compound channel flow are given in Czernuszenko et al (2007).

3.2. Bursting Phenomena

There is a consensus among researchers that a turbulent shear flow consists of a series of large-scale high-speed and low-speed regions, which extend almost throughout the flow depth (e.g. Yalin 1992, Nezu and Nakagawa 1993, Nezu 2005). The large-scale lengths in spanwise as well as in vertical directions are of varying flow depths, and transition from low-speed to high-speed regions is more gradual than the other way around.

If the instantaneous shear stress is sufficiently large at any point, then some mass of fluid rolls-up into an eddy. This process generates a circulation motion of fluid in the low-speed region; the high-speed fluid overtakes the eddy and the part of low-speed fluid forms an ejection. Thus the stress in the fluid is relieved and a burst-forming eddy is born. This eddy travels in the low-speed fluid region; its size continually increases as well as the mass of fluid. The continual upward displacement of fluid progressively decreases, whereas its size increases. After this stage, the enlarging eddy is conveyed downstream, it obtains a size approaching its nearness to the free surface, then the eddy interacts with the latter and finally it completely disintegrates. The above-described sequence of events, which occurs between the birth of an eddy and its break-up is called the bursting process (Kim and Moin 1986).

The bursting process is composed of a quasi-cyclic process of ejections and sweeps. The occurrence of bursts in all parts of the flow means the continual conversion of the energy of the mean flow into turbulence kinetic energy, which is dissipated in the movement of small eddies. As claimed by Schoppa and Hussain (2002), bursting is an indirect indicator of streaks, and the connections between streaks and near-wall vortices are the subject of numerous investigations. It is not clear how the streamwise vortices are generated. Probably the most common physical model of bursting phenomena is a horseshoe vortex, also known as hairpin vortex, a mechanism belonging to the category of parent-offspring regeneration (Schoppa and Hussain 2002). There have been numerous studies aimed at the confirmation of the horseshoe vortex, and among them the work of Moin and Kim (1985), devoted to open-channel flow, should be mentioned. They indicated the occurrence of horse-vortex structures by analyzing the vorticity vectors and vortex lines of instantaneous 3D vorticity fields. These structures are generated from the roll-up of sheets of transverse vorticity. Other mechanisms of vortex formation fall in the category of instability-based, i.e. involving local instability of a quasi steady base flow, without requiring the presence of parent vortices (Schoppa and Hussain 2000).

Bursting motions occur randomly in space and time, and an appropriate detection function is not well established, although several detection functions have been proposed so far. The greatest difficulties in establishing a detection method arise from their random character. One of the methods for detecting bursting phenomena

is the analysis of instantaneous Reynolds-stress by the so-called threshold Quadrant technique.

3.2.1. Conditional Statistics and the Conditional Sampling Technique

Conditional statistics and sampling of the turbulent stress terms mean that ensemble averages of the considered shear stresses are conducted as the function of two conditions: a condition on the sign of the fluctuating velocities composing the considered covariance, and a condition on the instantaneous amplitude of this covariance relative to its mean value (Nakagawa and Nezu 1981). Conditional statistics permits the detection of coherent structures in turbulent boundary layers. The method relies on measurements of instantaneous shear stress in the turbulent flow considered.

The non-dimensional instantaneous Reynolds-stress fluctuations defined by Eq. (4) are a subject of our interest and their probability density distributions are defined in the form of Eq. (5). Hence,

$$NRS_{uw} = -\frac{u(t)\,w(t)}{\overline{uw}}, \quad NRS_{uv} = -\frac{u(t)\,v(t)}{\overline{uv}}, \quad NRS_{vw} = -\frac{v(t)\,w(t)}{\overline{vw}}. \tag{4}$$

For the sake of simplicity, only the product $u(t)w(t)$ will be defined in the further course of this paper. Equation (5) is obtained from the variable transformation in the joint probability density function of the $u(t)$ and $w(t)$ components if $p(u,w)$ obeys the Gaussian distribution for which all cumulants are zero (for details see Nezu and Nakagawa 1993):

$$p\left(\frac{uw}{\overline{uw}}\right) = \frac{1}{\pi}\frac{|R|}{(1-R^2)^{1/2}}\exp\left(\frac{R^2}{1-R^2}\frac{uw}{\overline{uw}}\right)K_0\left(\left\|\frac{R}{1-R^2}\frac{uw}{\overline{uw}}\right\|\right), \tag{5}$$

where, K_0 is the zeroth-order modified Bessel function of the second kind and R is the correlation coefficient defined as

$$R = \frac{-\overline{uw}}{u'w'}, \qquad \text{where} \qquad u' = \sqrt{\overline{u^2}}, \quad w' = \sqrt{\overline{w^2}}. \tag{6}$$

The shape of this distribution is characterized by the peak at $uw = 0$, because the Bessel function approaches infinity at this point. Comparisons with the experimental results will be given later in the paper.

3.2.2. Application of the Conditional Quadrant Method to Reynolds Stresses

Quadrant analysis is applied to discriminate important instantaneous Reynolds stress or covariance term, i.e., the product of $-u(t)w(t)$. This product is sorted over the four regions called quadrants of the $u - w$ plane as it is shown in Fig. 2.

Similar sorting can be made for the horizontal, $u - v$, plane. Unfortunately, the above mentioned quadrant sorting cannot be used directly as a detection function for
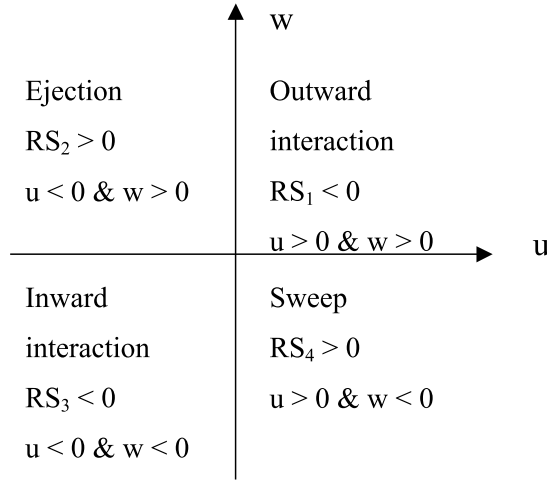
Fig. 2. Sketch for bursting events in $u - w$ plane for $H = 0$

bursting motions (for details see Nakagawa and Nezu 1993). For a better detection, a threshold level H is introduced and $u - w$ plane is divided into five regions. The additional region is called a 'hole', and is bounded by the curves $|uw| = Hu'w'$ in the plane $u - w$, where u' and w' are the local root-mean-square values of the u and w components of turbulent velocities. For $H \neq 0$, the quadrant events occur only if $|uw| > Hu'w'$, if not the 'hole' event is taken place. Basic definitions of all bursting events are given in Table 1 and Fig. 3.

Table 1. Basic definitions and notations for bursting events

Quadrant	Notation	$H = 0$	$H > 0$	Name	Direction
1	$QD - 1$	$u > 0$ and $w > 0$	$uw > Hu'w'$	Outward interaction	Upward front
2	$QD - 2$	$u < 0$ and $w > 0$	$-uw > Hu'w'$	Ejection	Upward back
3	$QD - 3$	$u < 0$ and $w < 0$	$uw > Hu'w'$	Inward interaction	Downward back
4	$QD - 4$	$u > 0$ and $w < 0$	$-uw > Hu'w'$	Sweep	Downward front
5	$QD - 5$	$-$	otherwise	Hole	$-$

Contributions to the total Reynolds stress or covariance term $\overline{uw}$, i.e. turbulent stress divided by ρ from the four quadrants, were computed from the following relationships:

$$RS_i = -\overline{uw_i} = \frac{-1}{N} \sum_{j=1}^{N} [uw_i(t)]_j, \quad \text{where} \quad uw_i(t) \quad \text{belongs to } i\text{-th quadrant,} \quad (7)$$

where RS_i is the fractional Reynolds stress belonging to the particular i-th quadrant, N is the total number of products $u(t)w(t)$.
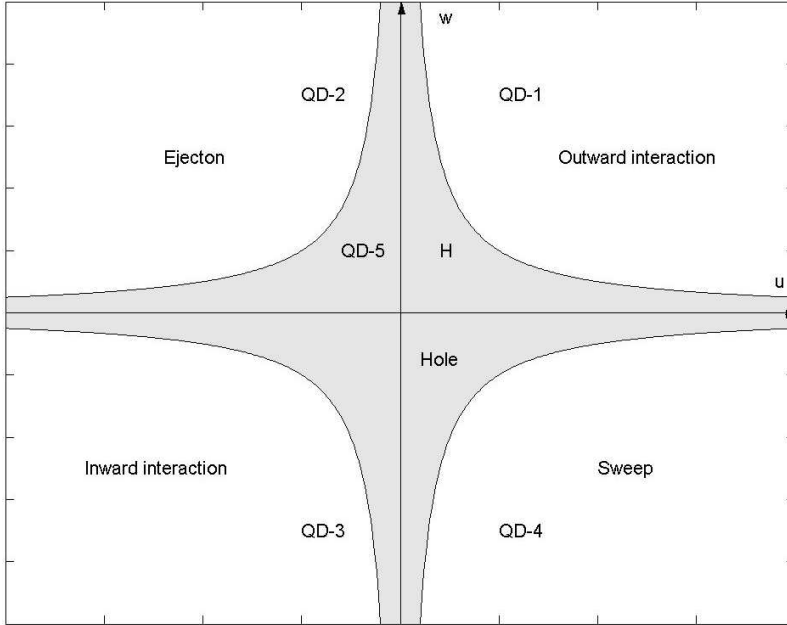
Fig. 3. Schematic division of bursting events including a threshold level H

The total normalized Reynolds stress is defined as

$$RS_{total} \equiv \frac{\tau}{\rho} = -\overline{uw} = \sum_{i=1}^{5} RS_i, \tag{8}$$

where RS_{total} is the total stress for the whole observation time related to the chosen pair of turbulent velocities.

3.2.3. Time Characteristics of Burst Events

The interpretation of turbulence structures is completed through the analysis of quadrant dominance in terms of mean and maximum residence time in each quadrant. For the examination of residence time, no threshold was applied and all events are taken into account. The process of counting the number of events related to the burst is highly problematic, because a definitive identification of bursts is required. When an event is not extremely violent, it is difficult to decide whether it is a burst or not. It is particularly troublesome in the measurements of the mean burst period from a single ADV signal, because only at one point in a complex bursting pattern

can the velocity be observed. Our attention is focused on the variation of the relative turbulent stress and the time fraction of events from the different quadrants as functions of the selection criteria. Thus the basic time characteristics for quadrant events are estimated by counting the number of times the conditions of particular events occur in a sequence − $T_{i,k}$. The mean and maximum residence time interval of the particular quadrant can be found along with the other time characteristics according to the following formulae:

$$\overline{T_i} = \frac{1}{N}\sum_{k=1}^{N} T_{i,k}, \quad T_{i,k} = n_{i,k}\,\Delta t,$$

$$T_{i,\max} = \max_{k\in(1,N)}(T_{i,k}); \quad P_i = \frac{T_i}{T} = \frac{n_i\Delta t}{N\,\Delta t}, \tag{9}$$

where $n_{i,k}$ is the number of occurrences in a sequence of events belonging to a particular quadrant − i, k is the number of particular events occurring in a sequence, Δt is the measuring fluctuating velocity time, P_i is the frequency of appearance of each quadrant, T_i is the total time of occurrences of a particular event, and N is the total number of observations.

4. Results and Discussion

4.1. Correlation Coefficient Distribution

The correlation coefficients between each of two turbulent velocity components measured in the main channel are defined by Eq. (6) and are shown in Fig. 4 as a function of non-dimensional distance from the bed. Correlation between longitudinal and vertical turbulent velocities, i.e. the ratio $(-\overline{uw}/u'w')$ does not change
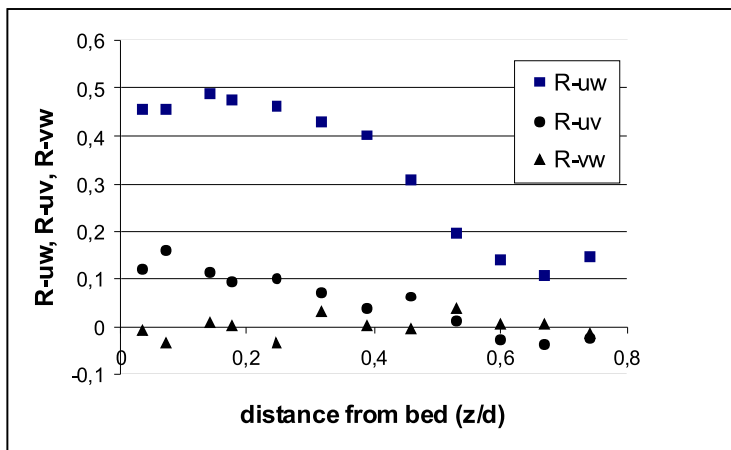

Fig. 4. Distribution of correlation coefficients in the main channel (vertical 39)

greatly until a distance of 0.3 of the channel depth is reached, at which point it begins to decrease. Lu and Wilmarth (1973) reported a value of 0.44 to 0.6 of the depth, which is a similar value to that obtained from measurements in our channel. In the greater part of the channel flows, the correlation coefficient is in the range between 0.4 to 0.5 as reported by others (this problem is discussed e.g. by Lu and Wilmarth 1973).

Fig. 4 shows that the values of correlation coefficient between the velocities $u(t)$ and $v(t)$ are rather small in comparison with the $u(t)$ and $w(t)$ components, and the values of $R - v(t)w(t)$, are even lower. Thus, the uw turbulent stresses will be the focus of our attention in the further course of the paper.

4.2. Probability Density Distributions of Turbulent Velocities

The probability density functions (pdf) of non-dimensional turbulent velocities defined as u_i/u_i' (subscript i stands for x, y and z directions, respectively) were calculated for selected verticals at several elevations. Figure 5 shows the pdf calculated for velocities measured at 1 cm from the bed, in the center of the main channel (vertical 39, $z = 1$ cm). The lateral turbulent velocity is seen to follow the normal
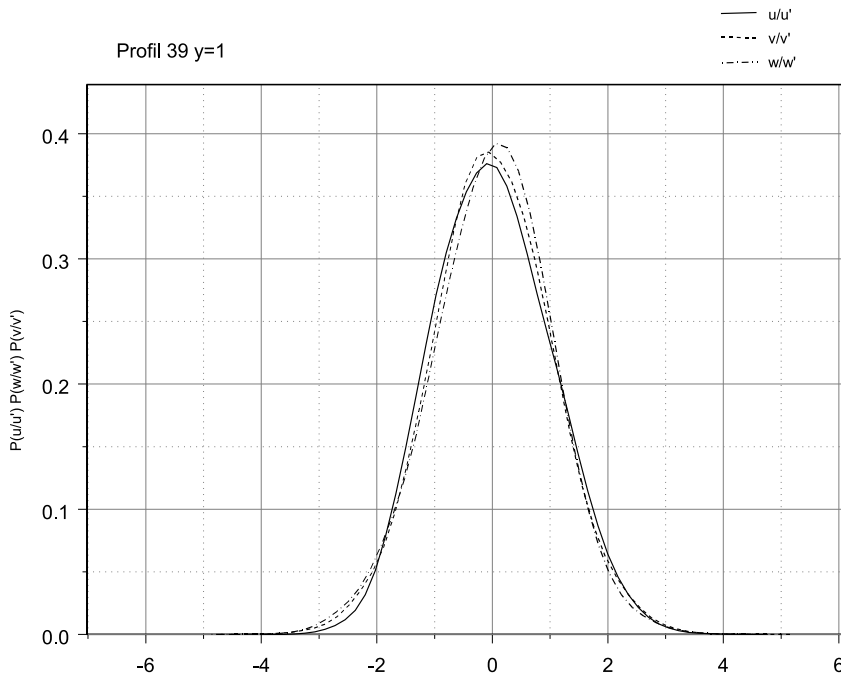

Fig. 5. Normalized probability density distributions: $p(u/u')$, $p(v/v')$ and $p(w/w')$ at vertical 39 at 1 cm from the channel bed

Gaussian distribution somewhat more closely than the remaining two components. The distribution of the longitudinal and vertical components are not so far from the Gaussian distribution; appropriate statistical characteristics for them are ($S_u = 0.15$, $D_u = -0.22$) and ($S_w = -0.11$, $D_w = 0.15$), where S denotes the skewness and D denotes the excess factors. More symmetrical distributions appear for larger distances from the bed, especially when transversal velocities are taken into account. In the case of longitudinal velocities, the kurtosis changes the sign from the negative to the positive, i.e. the peak of distribution becomes much sharper. This behaviour changes particularly above the inclined wall, where the agreement with the Gaussian distribution is much worse. An interesting feature is the change in sign of the skewness coefficient for the lateral velocities. Larger scatters between maximum and minimum values in the time series of non-dimensional turbulent velocities (u/u') are observed there and the differences between them are equal to 17 for $z/d = 0.74$ and 7 for $z/d = 0.05$ ($z = 1$ cm) (see Table 2). The kurtosis close to the water surface is much greater than those for the normal distribution (Table 2). This is caused by large scale horizontal motion created by large differences in the velocities between the main channel and the flood plane.

Table 2. Kurtosis, skewness, minimum and maximum values from 9000 values of standardized non-dimensional turbulent velocity distribution for verticals 39 and 34 and for two distances from the bed

	u/u'	w/w'	v/v'
Vertical 39 $z = 1$			
Kurtosis	−0.2183	0.1536	0.1395
Skewness	0.15454	−0.1142	0.03262
Minimum	−3.1990	−4.0182	−3.8364
Maximum	3.8782	3.9420	4.3163
Vertical 39 $z = 21$			
Kurtosis	1.8251	0.1239	0.1427
Skewness	0.1652	0.0561	−0.0034
Minimum	−7.4150	-3.5163	−4.0322
Maximum	9.5412	4.0272	4.0711
Vertical 34 $z = 1$			
Kurtosis	−0.2124	0.1602	0.2210
Skewness	−0.0311	0.0231	−0.0394
Minimum	−4.2011	−4.0910	−4.5968
Maximum	3.1142	3.6456	4.1220
Vertical 34 $z = 15$			
Kurtosis	0.0904	0.3637	0.2069
Skewness	−0.3370	0.3537	0.2022
Minimum	−4.8406	−3.5002	−4.0672
Maximum	2.9539	4.32892	4.2683

4.3. Probability Density Distributions of the Covariance Terms: $uw(t)$ and $u(t)v(t)$

The conditional quadrant method has been applied to describe the statistical properties of the covariance terms $u(t)w(t)$ (along the vertical plane) and $u(t)v(t)$ (along the horizontal plane). Our measurements as well as those of others (e.g. Hurther 2000) show that the term describing the statistical properties across the mean flow has equal contribution to the total stress for all quadrants, independently of the threshold level and water depth. Therefore, this covariance will not be discussed in the paper.

The typical calculated pdf for $u(t)w(t)$ in the main channel collapses well with the theoretical distribution based on Eq. 5 (Fig. 6a: vertical 39 at $z = 1$ cm, and Fig. 6b: vertical 39 at $z = 1$ cm). A very similar picture might be obtained for measuring points above the inclined walls. A common feature of those distributions is that they have long tails for extreme values of uw and sharp peaks at $uw = 0$.

### 4.4. Contribution to Reynolds Stresses from Different Events

Typical results of measurements of the contribution to Reynolds stresses from different events and different holes are shown in Figs 7 and 8.

As in the case of other characteristics, results for two verticals 39 and 34 are presented. Two distances from the bed have been selected, namely $z = 1$ cm and $z = 7$ cm. The largest contribution to the total Reynolds stresses – uw, comes from the second and the fourth quadrant (ejection and sweep). The ratio $(RS_2 + RS_4)/(RS_1 + RS_3)$ (RS_i denotes the stress computed for i-th quadrant only) ranges from about 5 near the wall to 1.5 near the water surface (Table 3). The difference between the ejection and the sweep contributions is not so large near the bed, for $z = 1$ cm, sweeps prevail, but for $z = 7$ cm the ejection has larger values. Generally, for large distances from the bed these differences are greater. Contributions from remaining quadrants to the total stress are negative and relatively small. When the hole size becomes large it turns out that there are only two contributions to the total stress, coming from the ejections and the sweeps (see Fig. 7).

Similar results are obtained for the uv covariance at a vertical located above the inclined wall. There are no differences between two even quadrants (QD-2 and QD-4) and two odd quadrants (QD-1 and QD-3) near the bed. For larger distances from the channel bed, the ejection prevails for all sizes of the assumed hole. The comparison of odd quadrants shows that the first quadrant prevails over the third one for larger distances from the bed (see Fig. 8).

The calculated fractional contributions to the total Reynolds stresses confirm that the ejections and sweeps prevail near the bed, and when the distance from the bed increases then their dominance becomes weaker and the contribution from different events becomes more uniformly distributed (despite their signs) among the quadrants (see Table 3). The total stress reaches its minimum value near the water
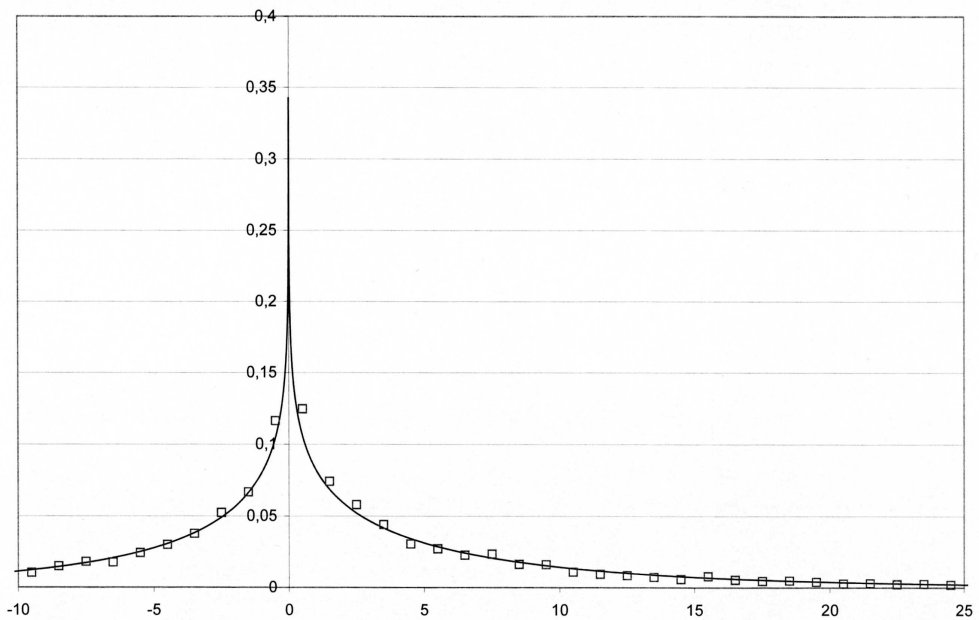
(a) T1V39_1
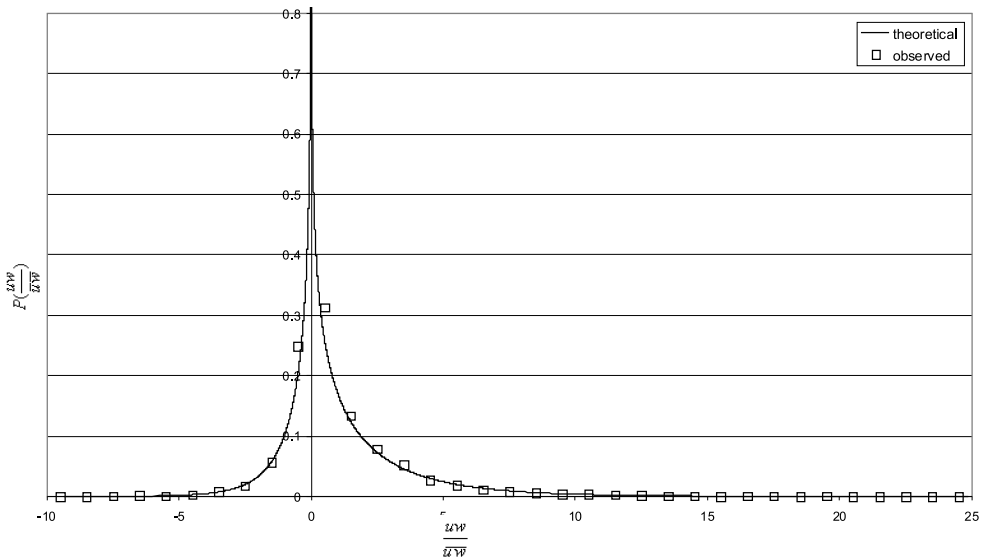
(b) T1V39_19

Fig. 6. Probability density distribution $p\,(uw(t)/\overline{uw})$ of the signal $uw(t)/\overline{uw}$ for main channel (vertical 39); (a) Test 1, vertical 39, $z = 1$ cm (T1V39_1) and (b) Test 1, vertical 39, $z = 19$ cm (T1V39_19). Solid line – Eq. (5), squares – calculated
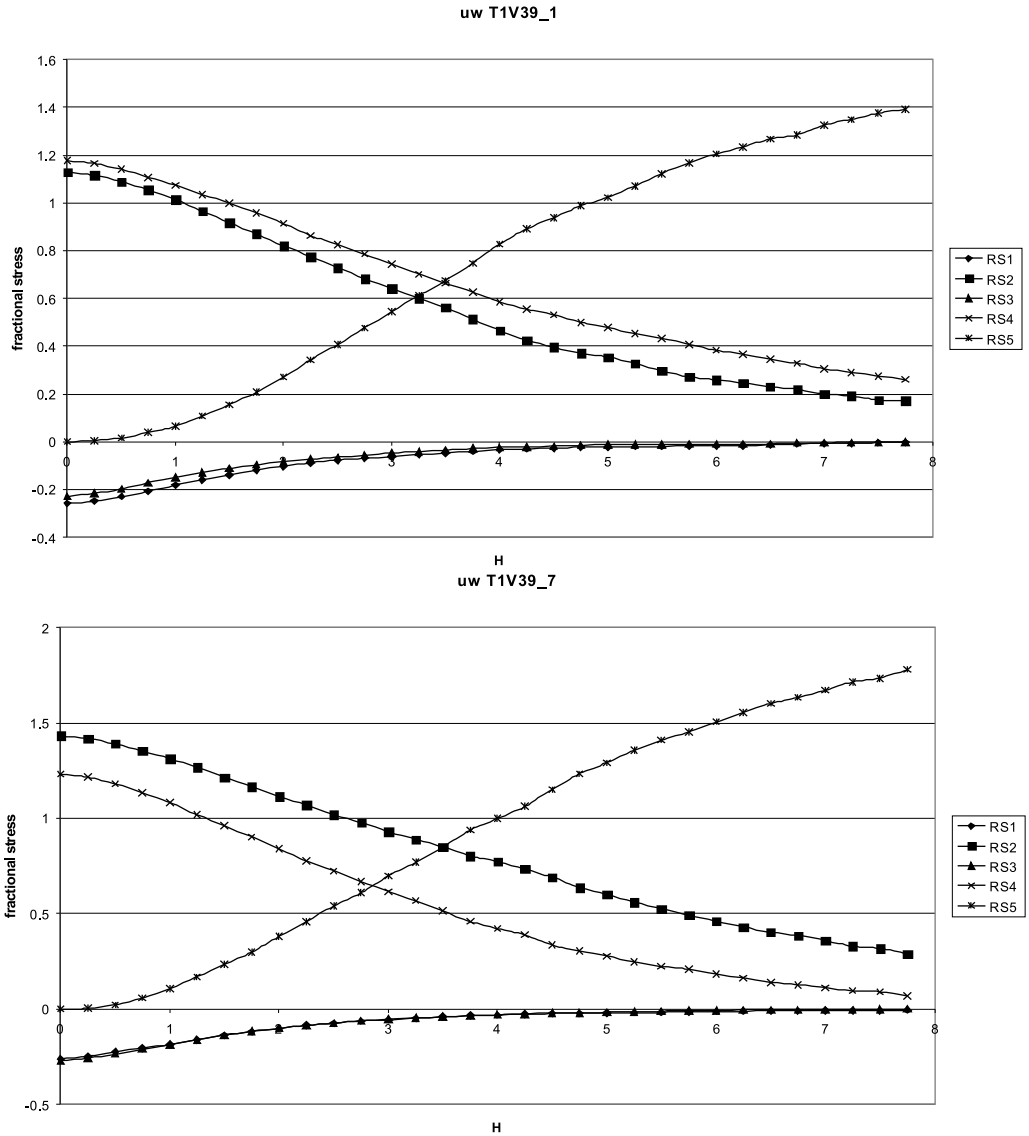
Fig. 7. Fractional contribution from i-quadrant (RS_i) to total Reynolds stresses $-\overline{uw}$ as a function of hole sizes for each quadrant in the main channel (vertical 39) at two distances from the bed: $z = 1$ cm and $z = 7$ cm
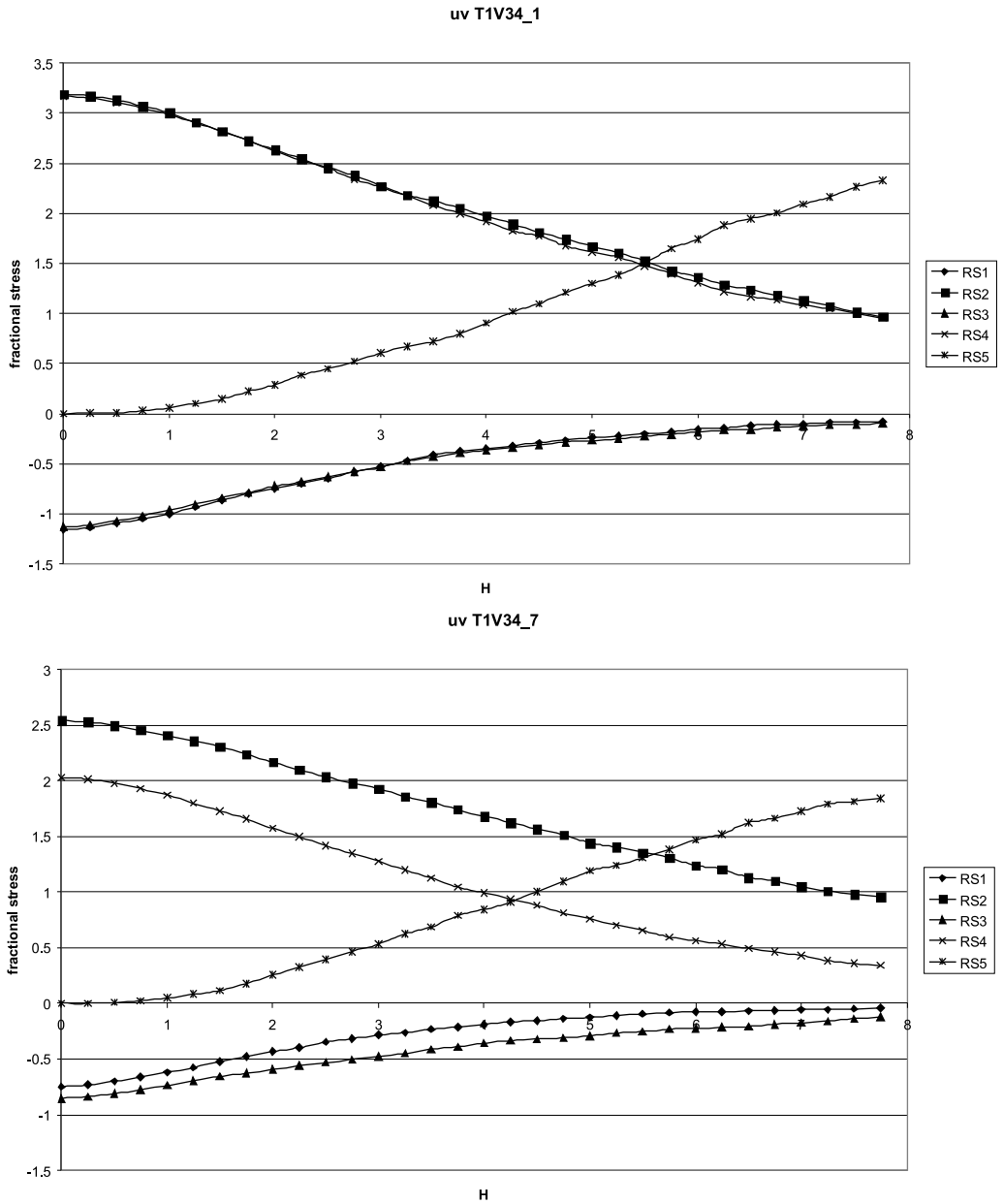
uv T1V34_1

uv T1V34_7

Fig. 8. Fractional contribution from *i*-quadrant to the total Reynolds stresses −*uv*, as a function of hole sizes over the inclined wall (vertical 34) at two distances from the bed: *z* = 1 cm and *z* = 7 cm

Table 3. Contribution to the total Reynolds stresses $-\overline{uw}$ from different events as a function of distances from the bed for two hole sizes: $H = 0$ and $H = 5$, for the main channel

$H = 0$ Z [cm]	RS_1 [(cm/s)^2]	RS_2 [(cm/s)^2]	RS_3 [(cm/s)^2]	RS_4 [(cm/s)^2]	$RS_2 + RS_4$ $(RS)_1 \ RS_3$ [(cm/s)^2]	RS_{total} [(cm/s)^2]
1	−0.259	1.129	−0.229	1.177	−4,725	1.818
2	−0.278	1.339	−0.29	1.383	−4,792	2.154
4	−0.279	1.545	−0.278	1.462	−5,259	2.450
5	−0.288	1.49	−0.289	1.387	−5,399	2.300
7	−0.261	1.432	−0.272	1.231	−4,986	2.130
9	−0.236	1.259	−0.271	0.878	−4,996	1.630
11	−0.204	1.022	−0.221	0.636	−4,215	1.233
13	−0.179	0.606	−0.19	0.41	−3,901	0.647
15	−0.171	0.431	−0.204	0.316	−2,753	0.372
17	−0.200	0.319	−0.183	0.281	−1,992	0.217
19	−0.209	0.283	−0.196	0.291	−1,567	0.169
21	−0.192	0.277	−0.178	0.307	−1,417	0.214

$H = 5$ Z [cm]	RS_1 [(cm/s)^2]	RS_2 [(cm/s)^2]	RS_3 [(cm/s)^2]	RS_4 [(cm/s)^2]	RS_5 [(cm/s)^2]	RS_{total} [(cm/s)^2]
1	−0.022	0.354	−0.013	0.477	1.022	1.818
2	−0.014	0.380	−0.018	0.503	1.303	2.154
4	−0.008	0.539	−0.011	0.398	1.532	2.450
5	−0.024	0.574	−0.017	0.401	1.366	2.300
7	−0.020	0.599	−0.017	0.277	1.291	2.130
9	−0.018	0.699	−0.029	0.170	0.807	1.629
11	−0.031	0.647	−0.031	0.123	0.527	1.235
13	−0.051	0.429	−0.054	0.156	0.166	0.646
15	−0.096	0.327	−0.102	0.186	0.037	0.352
17	−0.141	0.250	−0.118	0.209	0.015	0.215
19	−0.164	0.231	−0.148	0.242	0.009	0.170
21	−0.136	0.205	−0.114	0.239	0.019	0.213

surface: for example at $z = 19$ cm the total stress equals to 0.17 which is about 7% of its value at $z = 4$ cm.

When $H = 0$, one can say that near the bed ($z = 1$ cm) the sweeps prevail, and starting from $z = 3$ cm the ejections become larger, so that the difference $RS_2 − RS_4 = −0.048$ for $z = 1$ cm, and then it increases to a value of 0.38 for $z = 11$ cm, and again gradually decreases to −0.03 near the water surface (see Table 3). When the hole is large, e.g. $H = 5$, the values of the difference $RS_2 − RS_4$ are –0.123, 0.524 and –0.034 for $z = 1$ cm, $z = 3$ cm and $z = 11$ cm, respectively. It is easy to see that the differences between particular quadrants are more pronounced for larger sizes of the hole. Near the wall (till 5 cm), the sweeps and ejections contribute
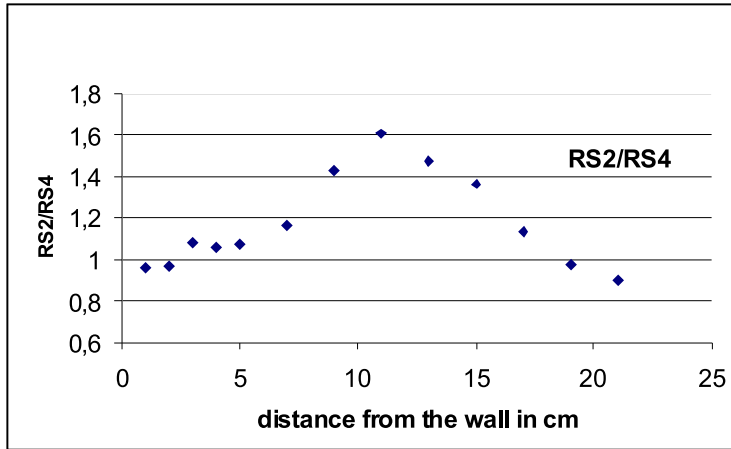
Fig. 9. Distribution of the ratio RS_2/RS for the main channel (vertical 39) with $H = 0$

almost equally to the total stress, then the relative ratio reaches its maximum value 1.6 in the middle part, and then it again gradually decreases to the value of 0.9 (see Figure 9). The above justifies to some extent the statement that the turbulence is almost totally generated near the bed within the ejections and sweeps, and the contributions of both events at $H = 0$ is about 85% when $H = 0$, and this increases to 98% when $H = 5$. Remember that in our case the data from the distance 15 cm above the bed are influenced by a horizontal large vortex, and cannot be compared with a common 2D situation.

To summarize, the contribution of the ejections and sweeps to the total stresses decreases when the distance from the bed increases, whereas the contribution of the remaining two quadrants increases.

4.5. Mean Periods and Scales of Burst Events

The average residence times of all events belonging to a particular quadrant were calculated for different distances from the bed and are shown in Fig. 10. The results of calculations of the maximum time interval of the particular events are displayed in Table 4.

Figure 10 shows that the average time of duration of the sweeps and ejections for $z/d < 0.2$ is about 0.12 s. In the case of two other events that value is by a half smaller, i.e. about 0.06 s. The mean time for the two major events decreases together with the increase of the distance from the bed until the value of $y/d = 0.5$ is reached. Then the mean time duration for all events is almost the same and equal to 0.075 s.

Calculations of the maximum duration (see Table 4) for all events show that these times are larger for even quadrants than those for odd quadrants. Comparing even quadrants, one can see that starting from $z = 1$ cm ($z/d = 0.035$) till $z = 9$ cm
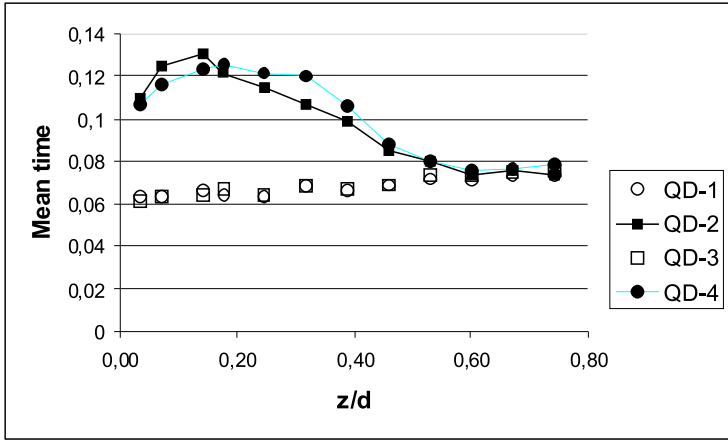
Fig. 10. Mean residence time in seconds for all quadrants of *uw* as a function of the distances from the bed (*z/d*) for the main channel for *H* = 0

Table 4. Maximum time periods for all quadrants, and scales for ejection and sweep as a function of the distances from the bed of the main channel (vertical 39)

z [cm]	z/d −	$QD-1$ [s]	$QD-2$ [s]	$QD-3$ [s]	$QD-4$ [s]	$L_{Q2,max}$ [cm]	$L_{Q4,max}$ [cm]
1	0.035	0.40	1.00	0.40	0.72	28.20	20.30
2	0.071	0.36	1.24	0.44	1.36	36.82	40.38
4	0.141	0.40	1.12	0.36	1.08	36.12	34.83
5	0.177	0.36	1.24	0.44	1.28	41.24	42.57
7	0.247	0.36	0.96	0.36	0.92	33.83	32.42
9	0.318	0.48	1.12	0.56	1.00	41.90	37.41
11	0.389	0.48	0.92	0.40	1.12	35.62	43.37
13	0.459	0.36	0.56	0.48	1.04	22.36	41.53
15	0.530	0.68	0.48	0.44	0.72	19.34	29.01
17	0.601	0.64	0.72	0.44	0.80	29.04	32.27
19	0.671	0.44	0.64	0.64	0.76	25.88	30.73
21	0.742	0.52	0.48	0.48	0.84	19.32	33.82

(*z/d* = 0.3) the maximum duration for both quadrants are similar, and after that the duration of the sweeps prevails over the ejections.

One can say that these times can be interpreted as the scales of a rough measure of the longest connection in the turbulent behavior of these structures. Also, it is possible to introduce the Eulerian length scale as the product of the local mean velocity and the maximum time duration, i.e.

$$L_{i,\max} = U_i T_{i,\max}. \tag{10}$$

This length represents the largest size of the ejections or sweeps at the considered distance from the bed. The largest sizes of the ejection and sweep are about 42 cm within the main part of the water depth (5–11 cm), but near the water surface they are lower (about 25–30 cm) (Table 4).

4.6. Frequency of Occurrence of Events

The frequency of occurrence of all kinds of considered events is shown in Figure 11 as a function of the normalized distance from the bed. It can be seen that the frequencies of occurrence of sweeps and ejections are much higher than the frequencies of the remaining events, which is particularly evident close to the bed (35% against 15%). It is worth noting that the frequency of all quadrant events approaches the value of 25% near the free water surface, which suggests that all the events are almost equal there. The total Reynolds shear stresses reach the minimum value at the surface. Sweeps reach their maximum value (approximately 0.35%) at the distances from the bed within the range of $0.2 < z/d < 0.4$, and the ejections become largest very close to the bed.
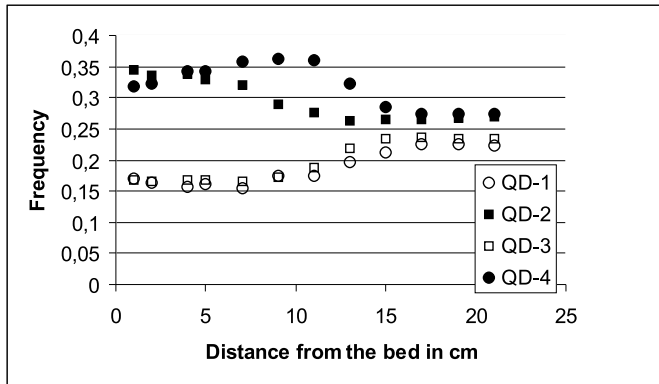

Fig. 11. Distribution of frequency of all events belonging to $-uw$ in the main channel (vertical 39)

4.7. The Angle of the Events

The angle of an individual event is defined as the angle of a vector of turbulent velocities with respect to the longitudinal axis. This is determined from the ratio of temporary components of turbulent velocity fluctuations and then averaged for all velocities belonging to this event, according to the following formula:

$$|\theta_i| = \arctan\left(\left|\frac{w_i(t)}{u_i(t)}\right|\right), \quad \text{where } i = 2 \text{ or } 4 \text{ quadrant,} \tag{11}$$
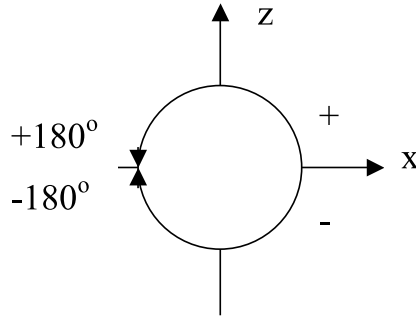
Fig. 12. Sign convention for sweep and ejection angles

where θ_i is the angle of the quadrant measured from the horizontal axis.

The sign convention for the sweep and ejection angles is shown in Figure 12. The angle of velocities related to the events of the ejection and sweep have a very important physical meaning and can, for example, be identified as the force acting upon sediment particles on the channel bed. The angle of velocities corresponding to the ejections and sweeps as a function of the normalized distance from the bed is shown in Table 5. For the ejection, the angle is in the range from 160° at $z = 1$ cm, then gradually decreases to 153° at 14 cm, and again increases to 158.6° at 21 cm from the bed. A similar pattern may be observed for the sweeps – their values start from –21°, go through –24.5° at 13 cm, and end at the value of –20.5°. Note that those angles for the ejections and sweeps are inclined differently in relation to the horizontal direction. Similar results were obtained by Keshavarzy and Ball (1997), where for the sweeps, the averaged angle started at –20°, and then gradually

Table 5. Angle of ejection and sweep events for main channel (vertical 39)

z [cm]	z/d	Sweep angle [degree]	Ejection angle [degree]
1	0.04	–20.94	159.25
2	0.07	–22.07	157.32
4	0.14	–23.79	156.31
5	0.18	–23.89	155.51
7	0.25	–23.23	155.40
9	0.32	–24.42	154.58
11	0.39	–24.04	154.45
13	0.46	–24.46	152.94
15	0.53	–24.05	153.21
17	0.60	–23.85	155.37
19	0.67	–22.73	157.10
21	0.74	–20.54	158.55

decreased to –30°, and for ejections those angles changed in the range from 160° to 150°.

5. Concluding Remarks

The results in the present paper show the basic properties of the coherent structures which were experimentally observed in a two-stage laboratory channel, and they may be summarized as follows:

1. The standardized probability density functions of non-dimensional turbulent velocity show that all the components of turbulent velocity follow, more or less, the normal Gaussian distribution. Larger deviation from the Gaussian distribution is found above the inclined wall, especially close to the water surface. These deviations come from the large scale of horizontal motion caused by the difference in velocities between the main channel and the floodplains.
2. The significance of the ejection and sweep in generating the turbulence near the wall and their contributions to the vertical component of the Reynolds stresses in the main channel is evident. The contributions from the remaining odd quadrants to the total stress are relatively small. A similar relation holds for covariance $u(t)v(t)$ at a vertical above the inclined wall. The significance of ejections increases in comparison with other events as the distance from the channel bed increases.
3. The average time of duration of sweeps and ejections in the wall region of flow is twice as great as of other events, averaging 0.12 s. It then decreases with the distance from the bed up to the flood plain level. Starting from some threshold value ($y/d = 0.6$), the mean time duration is the same for all events. The largest sizes of the ejections and sweeps are about 42 cm within the main part of the water depth, but near the water surface they are much lower (about 25–30 cm).
4. The frequencies of the occurrence of sweeps and ejections are higher than of other events, particularly in the wall region. These frequencies level out near the free water surface, and the total Reynolds shear stress reaches its minimum there.
5. The angle of velocity for the ejection starts from 160 degrees at the level $z = 1$ cm, and then gradually increases to 27.1° at the distance of 14 cm, and again decreases towards the value of 21.4 degrees at the distance of 21 cm from the bed. For the sweeps, those angles have a similar functional relationship and start from 21 degrees, achieving a maximum value of 24.5° at the distance of 13 cm from the bed, and end at the level of 20.5°.

Acknowledgments

References

Bogard D. G., Tiedermann W. G. (1986) Burst detection with single-point velocity measurements, *J. Fluid Mech.*, 162, 389–413.

Buffin-Bélanger T., Roy A. G. (2005) 1 min in the life of a river: selecting the optimal length for the measurement of turbulence in fluvial boundary layers, *Geomorphology*, 68, 77–94.

Czernuszenko W., Kozioł A., Rowiński P. M. (2007) Measurements of 3D Turbulence Structure in a Compound Channel, *Archives of Hydro-Engineering and Environmental Mechanics*, **54** (1), 55–73.

Czernuszenko W., Rowiński P. M. (2008) Reynolds stresses in a compound open channel flow – flume experiments, *International Conference on Fluvial Hydraulics, River Flow*, **1**, Cesme-Izmir, Turkey, 289–297.

Detert M., Weitbrech V., Jirka G. H. (2007) Simultaneous velocity and pressure measurements using PIV and multi layer pressure sensor arrays in gravel bed flows, *HMEM 2007*, ASCE – Conference, Lake Placid.

Franca M. J., Lemmin U. (2006) Detection and reconstruction of coherent structures based on wavelet multiresolution analysis, *River Flow 2006*, Ferreira, Alves, Leal and Cardoso (eds), Taylor and Francis Group, London, 181–188.

Grass A. J., Stuart R. J., Mansour-Tehrani M. (1993) Common vortical structure of turbulent flows over smooth and rough boundaries, *AIAA Journal*, **31** (5), 837–847.

Hurther D. (2000) Shear stress statistics and wall similarity analysis in turbulent boundary layers using a high resolution 3-D ADVP, *IEEE Journal of Oceanic Engineering*, **25** (4), 446–457.

Hyun B. S., Balachandar R., Yu K., Patel V. C. (2003) Assessment of PIV to measure mean velocity and turbulence in open-channel flow, *Experiments in Fluids* 35, 262–267.

Keshavarzy A., Ball J. E. (1997) An analysis of the characteristics of rough bed turbulent shear stresses in an open channel, *Stochastic Hydrology and Hydraulics*, 11, 193–210.

Kim J., Moin P. (1986) The structure of the vorticity field in turbulent channel flow: Part 2. Study of ensemble-averaged fields, *J. Fluid Mech.*, 162, 339–363.

Kumar S., Gupta R., Banerjee S. (1998) An experimental investigation of the characteristics of the free surface turbulence in channel flow, *Physics of Fluids*, **10** (2), 437–456.

Lohrmann A., Cabrera R., Kraus N. (1994) Acoustic-Doppler Velocimeter (ADV) for Laboratory Use, *Fundamentals and Advacements in Hydraulic Measurements and Experimentation*; Proc., Buffalo, New York: 351–365.

Lu S. S., Willmarth W. W. (1973) Measurements of the structure of the Reynolds stress in a turbulent layers, *J. Fluid Mech.*, 60, 481–511.

Moin P., Kim J. (1985) The structure of the vorticity field in turbulent channel flow: Part 1, Analysis of instantaneous fields and statistical correlations, *Journal of Fluid Mechanics* 155, 441–464.

Nakagawa H., Nezu I. (1977) Prediction of the contributions to the Reynolds stress from the bursting events in open channel flows, *J. Fluid Mech.*, 80, 99–128.

Nakagawa H., Nezu I. (1981) Structure of space-time correlations of bursting phenomena in an open-channel flows, *J. Fluid Mech.*, 104, 1–43.

Nezu I. (2005) Open-channel flow turbulence and its research prospect in the 21st century, *J. Hydraulic Eng., ASCE*, **131** (4), 229–246.

Nezu I., Nakagawa H. (1993) *Turbulence in Open-Channel Flows*, A. A. Balkema, Rotterdam.

Nikora V., Goring D. (2000) Flow turbulence over fixed and weakly mobile gravel beds, *J. Hydraulic Eng. ASCE*, **126** (9), 679–690.

Offen G. R., Kline S. J. (1975) A proposed model of the bursting process in turbulent boundary layers, *J. Fluid Mech.*, **70** (2), 209–228.

Prooijen B. C. van Battjes J. A., Uijtewaal S. J. (2005) Momentum exchange in straight uniform compound channel Flow, *J. Hydr. Engrg. ASCE*, **131** (3), 175–183.

Rowiński P. M., Czernuszenko W., Kozioł A. P., Kubrak J. (2002) Properties of a streamwise turbulent flow field in an open two-stage channel, *Archives of Hydro-Engineering and Environmental Mechanics*, **49** (2), 37–57.

Rowiński P. M., Mazurczyk A. (2006) Turbulent characteristics of flows through emergent vegetation. In *River Flow 2006* – Ferreira, Alves, Leal and Cardoso (eds), 2006 Taylor and Francis Group, London, 623–630.

Roy A. G., Buffin-Belanger T., Lamarre H., Kirkbride A. D. (2004) Size, shape and dynamics of large scale turbulent flow structures in a gravel bed river, *J. Fluid Mech.*, 500, 1–27.

Schoppa W., Hussain F. (2000) Generation of near-wall coherent structures in a turbulent boundary layer, *Current Science*, **79** (6), 849–858.

Schoppa W., Hussain F. (2002) Coherent structure generation in near-wall turbulence, *J. Fluid Mech.*, 453, 57–108.

Sumer B. M., Deigaard R. (1981) Particle motion near the bottom in turbulent flow in an open channel, Part 2, *J. Fluid Mech.*, 109, 331–337.

Yalin M. S. (1992) *River Mechanics*, Pergamon Press, Oxford.